Resolving Systematic Errors in Sulfate Source Apportionment: A Field-Validated Kinetic Isotope Fractionation Framework

Zhaobing Guo[1,2], Xuexue Bai[1], Qiwei Ai[1], Zizheng Xu[1], Shangshun Ma[1], Jiayu Gu[3], Pengxiang Qiu[1], and Qingjun Guo[4]

[1]Jiangsu Key Laboratory of Atmospheric Environment Monitoring and Pollution Control (AEMPC), Collaborative Innovation Centre of Atmospheric Environment and Equipment Technology (CIC-AEET), School of Environmental Science and Engineering, Nanjing University of Information Science and Technology, Nanjing 210044, China

[2]Suqian University, Suqian 223800 China

[3]School of Chemical Engineering and Materials, Changzhou Institute of Technology, Changzhou 213032, China

[4]Center for Environmental Remediation, Institute of Geographic Sciences and Natural Resources Research, Chinese Academy of Sciences, Beijing 100101, China

Correspondence to: Pengxiang Qiu (pxqiu@nuist.edu.cn) and Qingjun Guo (guoqj@igsnrr.ac.cn)

Abstract. Sulfates represent a critical constituent of atmospheric fine particulate matter ($PM_{2.5}$), significantly influencing air quality and climate dynamics. Precise quantification of atmospheric sulfate formation mechanisms and emission sources through stable isotope fractionation analysis represents a critical advancement in particulate matter pollution control. Conventional isotopic models relying on idealized complete SO_2 oxidation scenarios, while providing preliminary source apportionment estimates, exhibit systematic errors in reaction pathway quantification. Our field-validated approach incorporating actual atmospheric oxidation processes demonstrates that transition-metal ions (TMI)-catalyzed and NO_2-mediated pathways dominate sulfate production, with coal combustion (overestimate by ~~10.8~~10% in summer) and traffic emissions (underestimated by ~~8.2~~8% in summer) constituting primary sources. Comparative analysis reveals that traditional complete-oxidation models disproportionately diminish TMI pathway contributions, highlighting the necessity of kinetic fractionation corrections. These findings establish an improved isotopic tracing framework that resolves longstanding calculation discrepancies, delivering essential constraints for atmospheric sulfur cycle modeling and emission regulation strategies.

1 Introduction

Sulfate aerosols constitute a critical fraction of atmospheric particulate matter, with their formation mechanisms representing a pivotal yet unresolved aspect of air pollution control (He et al., 2012; Wang et al., 2018; Dao et al., 2019; Tao et al., 2016; Chen et al., 2023; Yu et al., 2026). The oxidation processes of sulfur dioxide (SO_2) exhibit remarkable mechanistic complexity stemming from its dual physicochemical nature (Kang et al., 2016; Mukai et al., 2001; Ma et al., 2025). The exceptionally high hydration equilibrium constant drives near-instantaneous formation of S(IV) species (HSO_3^-/SO_3^{2-}) (Zhang et al., 2026), while the thermodynamically favorable oxidation potential creates a multidimensional reaction pathways including both homogeneous radical processes and heterogeneous interfacial reactions (He et al., 2018; Harris et al., 2013b; Tanaka et al., 1994;

Zhang and Chan, 2023). These intrinsic reaction dynamics, when coupled with the extreme spatiotemporal variability of atmospheric conditions, create substantial obstacles for mechanistic elucidation under ambient environments. Current investigative approaches, including controlled laboratory simulations, field measurement, and computational modeling, each face inherent limitations when applied in isolation. Laboratory studies inevitably simplify the unbounded nature of atmospheric systems, while field observations struggle to isolate specific chemical processes amid complex real-world interactions. Modeling studies (Yang et al., 2025; 25 Zheng et al., 2024; Lin et al., 2022, 2025), though valuable for hypothesis testing, remain constrained by incomplete mechanistic understanding and parameterization challenges. This methodological trilemma has resulted in persistent knowledge gaps regarding the dominant pathways and quantitative contributions of various sulfate formation mechanisms in different atmospheric regimes.

The application of stable isotope techniques in sulfate source attribution has emerged as a powerful analytical approach, leveraging the distinct isotopic fingerprints characteristic of different pollution sources and their remarkable stability during atmospheric transport 2 (Yang et al., 2025; Lin et al., 2022; Harris et al., 2012b; Guo et al., 2024). This methodology capitalizes on the system-specific fractionation patterns inherent to various sulfate formation pathways, which serve as critical tracers for reconstructing oxidation mechanisms. Contemporary research has quantitatively established the sulfur isotopic signatures ($\delta^{34}S$) (Han et al., 2022; Yang et al., 2025) associated with major atmospheric oxidation routes, including transition metal ion-catalyzed (TMI, ~~$\delta^{34}S = a$~~), ozone-mediated (O_3 , ~~$\delta^{34}S = b$~~), nitrogen oxide-driven (NO_x ~~$\delta^{34}S = c$~~), and hydrogen peroxide-initiated (H_2O_2, ~~$\delta^{34}S = b$~~) pathways, through systematic analysis of particulate matter samples (Yang et al., 2025; Fan et al., 2020a; Harris et al., 2013a; Guo et al., 2019; Ruan et al., 2025; Wang et al., 2016; Wang et al., 2020). Advanced ~~mixing models,~~ analytical tools, particularly Bayesian isotopic mixing ~~approaches~~ and Rayleigh fractionation ~~formulations~~ models, have demonstrated ~~considerable~~ substantial utility in deconvoluting complex sulfate ~~sources and~~ formation mechanisms. Yet, their diagnostic potential is often overshadowed by a fundamental theoretical flaw: the reliance on complete SO_2 oxidation paradigms. Because genuine atmospheric regimes rarely achieve such idealized conversion, this oversimplification severely penalizes the accuracy of sulfur transformation kinetics. Ultimately, conventional Rayleigh approaches introduce systematic uncertainties into source apportionment by neglecting the vital kinetic isotope effects and partial intermediates generated during incomplete SO_2 processing.

~~Drawing conceptual inspiration from~~ Building upon these insights, the present study ~~pioneers a~~ establishes a comprehensive multi-model analytical framework that synergistically ~~combines~~ couples ambient field observations with ~~backward trajectory analysis~~ a suite of diagnostic tools, ranging from backward trajectory analysis to Bayesian isotope mixing models and process-specific Rayleigh fractionation modeling. This integrated approach achieves precision in quantifying sulfate formation pathways while systematically addressing the critical but often neglected kinetic limitations inherent to incomplete SO_2 oxidation under real atmospheric conditions. By applying ~~sulfur-oxygen~~ sulfur and oxygen isotope analyses to seasonally resolved aerosol samples from Nanjing, we demonstrate significant divergence between conventional complete-oxidation Rayleigh models

and our kinetic fractionation-corrected framework. ~~The~~ Our systematic model intercomparison ~~reveals substantial calibration~~ highlights the essential calibration requirements for stable isotope fractionation, ~~effects that have persistently biased previous sulfate source attribution studies.~~ successfully resolving the systematic biases that have long plagued sulfate source attribution. This methodological leap provides a refined method for tracking urban sulfate pollution, particularly within complex environments characterized by incomplete oxidation. Ultimately, the seasonally partitioned data from Nanjing serves as a quantitative benchmark, explicitly detailing how traditional complete-oxidation frameworks misrepresent source contributions during both summer photochemical and winter coal-combustion episodes.

2 Materials and methods

2.1 Sampling Sites

The atmospheric sampling protocol employed a monitoring site (118°43′E, 32°12′N) (Fig. S1) capturing seasonal extremes through January (winter) and July (summer) observations. A modified TH1000H high-volume sampler (Wuhan Tianhong Instrument) incorporated a dual-layer filtration assembly enabling concurrent $PM_{2.5}$ and SO_2 collection through co-laminated quartz (203×254 mm) and alkali-impregnated glass fiber filters (203×254 mm). Pre-treatment protocols involved muffle furnace combustion (~~450°C~~ 723 K for 2 h) followed by immersion in 2% K_2CO_3 + 2% glycerol solution for glass fiber filters. Sampling operations maintained 1.05 ~~$m^3 \cdot min^{-1}$~~ $m^3\ min^{-1}$ flow rates during 24-hour cycles ~~(08:00–08:00 local time)~~ with meteorological parameters (wind speed/direction, temperature, pressure, humidity) continuously logged. Post-sampling handling included foil-wrapping (pre-combusted ~~450°C~~ 723 K) followed by 24-hour desiccation and dark refrigeration. The final dataset comprised samples after excluding precipitation events, with quartz filters positioned upstream for particulate collection and treated glass fiber membranes downstream for gaseous SO_2 capture.

2.2 Sample Collection

The ionic composition analysis of $PM_{2.5}$ samples was performed using Dionex ICS-3000 and ICS-2000 ion chromatography systems (Thermo Fisher Scientific) for simultaneous determination of major water-soluble ions. The analytical suite comprised five cations (Na^+, NH_4^+, K^+, Mg^{2+}, Ca^{2+}) and three anions (Cl^-, NO_3^-, SO_4^{2-}). ~~The $\delta^{34}S$ value of sulfate was determined by precipitating $BaSO_4$ via $BaCl_2$ addition, followed by selective dissolution of residual $BaSO_3$ with 1 MHCl.~~ For the determination of sulfate $\delta^{34}S$ values, water-soluble sulfate within the filter extracts was initially isolated as $BaSO_4$ through the addition of an excess $BaCl_2$ solution. Because the sampling matrix inevitably captures both sulfate and sulfite, the latter originating from ambient SO_2, a targeted purification protocol was introduced; specifically, treating the co-precipitate with 1 M HCl selectively dissolved any residual $BaSO_3$ while leaving the acid-insoluble $BaSO_4$ intact. Following collection via filtration, the purified precipitate was rinsed thoroughly with deionized water until completely free of chloride ions and subsequently dried.

To eliminate potential organic interferences prior to isotopic interrogation, the dried $BaSO_4$ underwent thermal treatment in a muffle furnace at 1073 K for 2 hours. ~~Sulfur-oxygen isotope analysis~~ Sulfur and oxygen isotope ratios were determined by elemental analyzer (EA, Flash 2000, Thermo) combined with isotope mass spectrometer (IRMS, Delta V Plus, Finningan). Since $BaSO_4$ is an analytical sample for the determination of sulfur and oxygen isotope values in sulfate, the determination of sulfur isotope is to thermally decompose $BaSO_4$ and Cu_2O in a vacuum state, and use the generated SO_2 to analyze in a mass spectrometer (Yanagisawa and Sakai, 1983). In the determination of oxygen isotope, $BaSO_4$ was pyrolyzed by graphite furnace at 1723 K, and the oxygen isotope value of CO produced was measured in continuous flow mode (Mizutani and Rafter, 1969). The oxygen isotope in water was determined by the automatic carbon dioxide-water equilibrium method.

To ensure robust data quality, the analytical precision for all major water-soluble ions was rigorously verified via replicate measurements, consistently yielding values better than 5%. For the isotopic composition, results are reported in standard delta notation relative to international reference scales, specifically, Vienna Canyon Diablo Troilite (V-CDT) for $\delta^{34}S$ and Vienna Standard Mean Ocean Water (V-SMOW) for $\delta^{18}O$, as formulated in Eq. (1) and (2). Notably, our analytical system demonstrated high stability, with long-term reproducibility constrained to better than 0.2‰ and 0.3‰ for sulfur and oxygen isotopes, respectively.

$$\delta^{34}S(‰) = \left[\left({}^{34}S/{}^{32}S\right)_{sample}/\left({}^{34}S/{}^{32}S\right)_{reference} - 1\right] \times 1000 \quad (1)$$

$$\delta^{18}O(‰) = \left[\left({}^{18}O/{}^{16}O\right)_{sample}/\left({}^{18}O/{}^{16}O\right)_{reference} - 1\right] \times 1000 \quad (2)$$

Meteorological parameters and criteria air pollutant concentrations were acquired from two authoritative national databases during the sampling campaign. The China Meteorological Administration Data Service Center (https://data.cma.cn) provided comprehensive weather records, while real-time air quality metrics were retrieved from the China National Environmental Monitoring Centre's online platform (www.aqistudy.cn/), representing the official monitoring network for atmospheric composition surveillance.

2.3 ~~Trajectory Analysis Methodology~~ Air Mass Back Trajectories and Identification of Source Regions

~~The source apportionment and transport pathways of $PM_{2.5}$ were investigated using the HYSPLIT 4.0 backward trajectory model developed by NOAA's Air Resources Laboratory (ARL). This analysis integrated the FNL meteorological database to reconstruct air mass movements. For each analysis period, trajectories were initialized at 500 m above ground level with a 72-hour temporal window. Four trajectories per day were computed at 6-hour intervals (00:00, 06:00, 12:00, and 18:00) to capture diurnal variations in atmospheric transport patterns.~~ We conducted analysis of air mass back trajectories (Supporting Information Figures S3 and S4). The potential source regions were identified with (a) cluster analysis, (b) fractional cluster contributions, and (c) concentrated weighted trajectory (CWT) analysis of sulfate concentrations (Lin et al., 2022; Dasari et al., 2020; Fan et al., 2023) (methodological details in Supporting Information text S2).

2.4 Bayesian Stable Isotope Mixing Model

The source apportionment of sulfate aerosols was conducted through Stable Isotope Analysis in R (SIAR) modeling, a Bayesian framework that probabilistically quantifies contribution distributions and associated uncertainties from multiple emission sources by processing ambient δ^{34}S-SO_4^{2-} measurements (4) alongside source-specific δ^{34}S signatures of precursor sulfur gases with all environmental samples maintaining consistent natural properties to eliminate cross-data variability particularly seasonal δ^{34}S-SO_4^{2-} fluctuations where the winter dataset (n=16) and summer dataset (n=15) were separately processed through SIAR to establish seasonally resolved sulfate source profiles for the Nanjing region.

The SIAR model determines the probability distribution of source contributions to mixtures and uncertainties associated with multiple sources (Fan et al., 2020a; Zheng et al., 2024; Harris et al., 2012a). In the SIAR framework, the isotopic value j in species i (X_{ij}) is expressed as:

$$X_{ij} = \frac{\sum_{k=1}^{k} p_k q_{jk} (S_{jk} + C_{jk})}{\sum_{k=1}^{k} p_k q_{jk}} + \varepsilon_{ij} \quad (3)$$

$$S_{jk} \sim N(\mu_{jk}, \omega_{jk}^2) \quad (4)$$

$$C_{jk} = (\lambda_{jk}, \tau_{jk}^2) \quad (5)$$

$$\varepsilon_{ij} \sim (0, \sigma_j^2) \quad (6)$$

Where q_{jk} is isotopic value j in source; S_{jk} is source k for isotope j, normally distributed with mean (μ_{jk}) and variance (ω_{jk}^2); C_{jk} is isotopic enrichment factor for isotope j in source k, normally distributed with mean (λ_{jk}) and variance (τ_{jk}^2); p_k is proportion of source k; ε_{ij} is residual error representing unquantified variation between individual species, normally distributed with mean (0) and variance (σ_j^2).

2.5 Relative Contributions of SO_2 Oxidation Pathways to Sulfate Aerosols

Four sulfate formation pathways were considered: OH, H_2O_2/O_3, TMI, and NO_2 oxidation. Given the similar fractionation factors of H_2O_2 and O_3 (Harris et al., 2012a, b; Lin et al., 2022), we used $\alpha(H_2O_2/O_3)$ to represent their combined fractionation. The temperature-independent α^{34}S fractionation factors are calculated as (Lin et al., 2022; Fan et al., 2020b):

$$\alpha^{34}S_{OH}(‰) = -(0.004 \pm 0.015) \times T + (10.60 \pm 0.73) \quad (7)$$

$$\alpha^{34}S_{H_2O_2/O_3}(‰) = -(0.085 \pm 0.004) \times T + (16.51 \pm 0.15) \quad (8)$$

$$\alpha^{34}S_{TMI}(‰) = -(0.237 \pm 0.004) \times T + (-5.039 \pm 0.044) \quad (9)$$

$$\alpha^{34}S_{NO_2}(‰) = exp\,[(0.2437 \pm 0.0457)/T + (0.0008 \pm 0.019)] \quad (10)$$

Where T is ambient temperature (°C). The total α^{34}S fractionation is computed as (Fan et al., 2020b; Harris et al., 2013a):

$$\alpha^{34}S = f_{OH} \times \alpha^{34}S_{OH} + f_{H_2O_2/O_3} \times \alpha^{34}S_{H_2O_2/O_3} + f_{TMI} \times \alpha^{34}S_{TMI} + f_{NO_2} \times \alpha^{34}S_{NO_2} \quad (11)$$

Where f_{OH}, $f_{H_2O_2/O_3}$, f_{TMI} and f_{NO_2} denote relative fractions of sulfate production from respective pathways, constrained by $\sum f_x = 1$.

2.6 Sulfur Isotope Fractionation Modeling via Rayleigh Fractionation

Due to the absence of sulfur isotope equilibrium between atmospheric SO_2 and SO_4^{2-}, the Rayleigh Fractionation model can be applied to calculate the sulfur isotope fractionation effects between them. Within this framework, the $\delta^{34}S$ value of residual atmospheric SO_2 ($\delta^{34}S$-SO_2) is described by (Zheng et al., 2024; Lin et al., 2022):

$$\delta^{34}\text{S-SO}_2 = \delta^{34}\text{S-SO}_{2\text{-emission}} + \alpha^{34}S_{g\to p} \times ln\,(1 - \text{SOR}) \quad (12)$$

Where $\alpha^{34}S_{g\to p}$ denotes the fractionation factor for SO_2 (gaseous) → SO_4^{2-} (particles) conversion through gas and aqueous phases, $\delta^{34}\text{S-SO}_{2\text{-emission}}$ represents the $\delta^{34}S$ value of emission sources, and SOR is the SO_2 oxidation ratio, which can be calculated by the molar mass of SO_2 and SO_4^{2-}:

$$\text{SOR} = \frac{m(\text{SO}_4^{2-})/M(\text{SO}_4^{2-})}{m(\text{SO}_2)/M(\text{SO}_2)+m(\text{SO}_4^{2-})/M(\text{SO}_4^{2-})} \quad (13)$$

The source $\delta^{34}S$ value can be estimated from isotopic mass balance:

$$\delta^{34}\text{S-SO}_{2\text{-emission}} = \delta^{34}\text{S-SO}_2 \times (1 - SOR) + \delta^{34}\text{S-SO}_4^{2-} \times \text{SOR} \quad (14)$$

Where $\delta^{34}\text{S-SO}_4^{2-}$ is the observed $\delta^{34}S$ in sulfate. When SOR approaches 1 (complete SO_2 oxidation), $\delta^{34}\text{S-SO}_{2\text{-emission}}$ equals $\delta^{34}\text{S-SO}_4^{2-}$. The fractionation effects α is derived by combining Eq. (14) and (15):

$$\alpha_{g\to p} = \frac{(\delta^{34}\text{S-SO}_{2\text{-emission}} - \delta^{34}\text{S-SO}_4^{2-}) \times \text{SOR}}{(1-\text{SOR}) \times ln\,(1-\text{SOR})} \quad (15)$$

~~To better understand this formula, we conducted α comparative analysis. The first scenario assumes Incomplete Oxidation Process of SO_2 (InCO Process) (SOR<1, partial conversion to SO_4^{2-}). The second scenario assumes Complete Oxidation Process of SO_2 (CO Process) (SOR=1, complete conversion to SO_4^{2-}).~~ The Complete Oxidation (CO) Process acts as an idealized baseline, operating on the premise that all gaseous SO_2 is exhaustively converted to particulate sulfate, yielding a sulfur oxidation ratio (SOR) of 1. Consequently, this framework directly equates the calculated source isotopic signature (δ^{34}S-source) to the measured sulfate value ($\delta^{34}\text{S-SO}_4^{2-}$), intentionally omitting the isotopic fractionation kinetics that govern the oxidation pathway. In contrast, the Incomplete Oxidation (InCO) Process reflects actual atmospheric conditions, specifically the reality that SO_2-to-sulfate conversion is inherently partial (SOR < 1). Grounded in the Rayleigh fractionation model, this framework synchronously integrates the observed isotopic values of gaseous SO_2 and particulate SO_4^{2-} with the corresponding SOR. By doing so, it inversely derives more realistic source isotopic signatures alongside the kinetic fractionation factors (α), a conceptual advancement that forms the core innovation of our study.

2.7 Estimation of primary sulfate and secondary sulfate

The underestimation of primary sulfate emissions can partially account for the phenomenon known as missing sulfates (Ding et al., 2021). The anthropogenic primary sulfate is estimated as 3% of anthropogenic sources of sulfur emissions in the model (Alexander et al., 2009). Assuming all the detected concentrations of SO_2 and precursors of secondary sulfate are anthropogenic, we can deduce Eq. (17). Considering the influence of anthropogenic sulfate sources on primary sulfate (He et al., 2018), the method for estimating primary sulfate can be expressed as follows:

$$n_{ps} = n_{ss} + n_{ts} + n_{ap} \quad (16)$$

$$n_{ap} = 3\% \times (n_{SO_2} + n_{sas}) \quad (17)$$

$$n_{sas} = n_{tos} - n_{ss} - n_{ts} - n_{ap} \quad (18)$$

Where n_{tos}, n_{ps} and n_{sas} represent the molar concentrations of the total primary, and secondary atmospheric sulfate, respectively, with the primary fraction further resolved into sea-salt (n_{ss}), terrestrial (n_{ts}), and anthropogenic primary (n_{ap}) components. To constrain these natural backgrounds, we employed companion tracer concentrations and mass ratios; specifically, sea-salt sulfate was quantified from soluble Na^+ assuming a purely marine origin (n_{ss} = k[Na^+], where k = [SO_4^{2-}]/[Na^+] = 0.25) (Zheng et al., 2024; He et al., 2018), while terrestrial sulfate was evaluated based on crustal Ca^{2+} abundances (0.18 × [Ca^{2+}]) (Zheng et al., 2024; He et al., 2018; Dasari et al., 2022; Dasari and Widory, 2024). Building upon this physical allocation, the stable sulfur isotope signatures ($\delta^{34}S$) are integrated via an isotopic mass-balance framework to isolate the secondary formation pathways (Zheng et al., 2024):

$$\delta^{34}S_{obs} = f_{ss} \times \delta^{34}S_{ss} + f_{ts} \times \delta^{34}S_{ts} + f_{ap} \times \delta^{34}S_{ap} + f_{sas} \times \delta^{34}S_{sas} \quad (19)$$

$$f_{ps} = f_{ss} + f_{ts} + f_{ap} \quad (20)$$

Here, $\delta^{34}S_{obs}$ denotes the bulk observed $\delta^{34}S$-SO_4^{2-} value, while the terms prefixed with f represent the corresponding molar fractions of each discrete source relative to the total sulfate burden, matched with their respective endmember isotopic signatures where f_{ps}, f_{ss}, f_{ts}, f_{ap}, and f_{sas} are the proportion of primary sulfate, sea salt sulfate, terrestrial sulfate, anthropogenic primary sulfate, and secondary sulfate, respectively ($\delta^{34}S_{obs}$, $\delta^{34}S_{ss}$, $\delta^{34}S_{ts}$, $\delta^{34}S_{ap}$, and $\delta^{34}S_{sas}$).

3 Results and Discussion

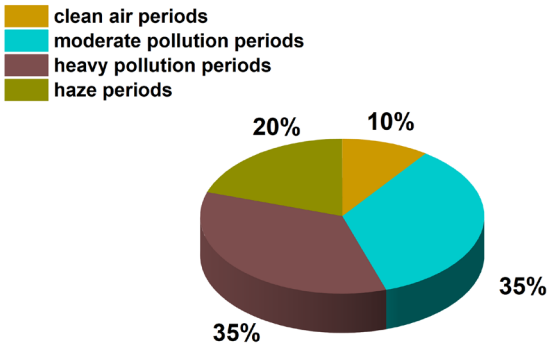

Figure 1. Proportion of different air mass periods

~~The~~ Chemical ~~characterization of $PM_{2.5}$~~ profiling of fine particulate matter in Nanjing reveals that ~~identified sulfate (SO_4^{2-}) as the predominant water-soluble inorganic ion , comprising~~ sulfate dictates the water-soluble inorganic fraction, accounting for ~~27.9% – 42.3%~~ 27.9% to 42.3% of the total ionic mass ~~fraction, a finding that underscores persistent sulfate-driven aerosol pollution in the region.~~ This pronounced dominance explicitly underscores the region's persistent susceptibility to sulfate-driven aerosol pollution. This pattern aligns with observations from other Chinese urban centers including Hangzhou (33.7%) (Lin et al., 2022), Guangzhou (40.2%-61.0%) (Tao et al., 2014b), and Beijing (33.0%) (Wei et al.,2018), collectively highlighting the prevalence of sulfate-rich $PM_{2.5}$ across China. Pollution episodes were categorized by $PM_{2.5}$ concentrations into clean (≤ 35 μg m^{-3}), moderate (35-75 μg m^{-3}), heavy (75-150 μg m^{-3}), and haze (> 150 μg m^{-3}) periods, with haze frequency (20%, Fig. 1) doubling that of clean periods (10%). Sulfate concentrations exhibited pronounced pollution-dependence, peaking at (27.55 ± 14.36 μg m^{-3}) during haze events 3.2 times higher than clean-phase levels (8.56 ± 3.19 μg m^{-3}).

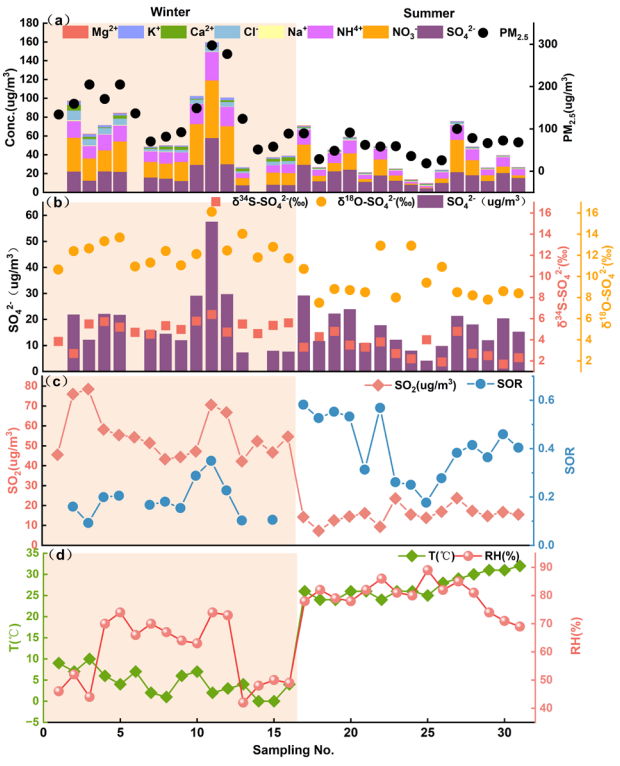

Figure 2. Time series of concentrations (values) of (a) $PM_{2.5}$ and ions, (b) SO_4^{2-} and $\delta^{34}S-SO_4^{2-}$, $\delta^{18}O-SO_4^{2-}$, (c) SO_2 and SOR, and (d) ambient temperature (*T*) and RH.

NH_4^+ and NO_3^- jointly accounted for 50.1%-57.9% of water-soluble ions (Fig. 2a), while their strong covariation with SO_4^{2-} (Fig. 2a, b) substantiates secondary sulfate formation as the principal $PM_{2.5}$ component and implicates combustion-derived emissions as its dominant source. The significant positive correlation between SO_4^{2-} and $PM_{2.5}$ concentrations (Fig. ~~S3~~S2) further establishes sulfate's direct mechanistic role in particulate pollution escalation. The atmospheric source apportionment can be quantitatively assessed through the $[NO_3^-]/[SO_4^{2-}]$ mass ratio, where elevated values reflect increasing dominance of mobile versus stationary emission sources (Xiao et al., 2014; Arimoto et al., 1996). Our measurements yielded ratios spanning 0.15-1.95 (mean 0.98 ± 0.42), exceeding Shanghai's 2002 baseline (0.43) (Yao et al., 2002) yet remaining below Jiaozuo's 2017 levels (1.36) (Zheng et al., 2024), collectively demonstrating Nanjing's intermediate position in mobile-source contribution among Chinese cities. These secondary aerosols originate through atmospheric oxidation of precursor gases, with SO_2 and NO_x principally derived from coal combustion and vehicular emissions respectively, while NH_3 predominantly stems from agricultural and livestock activities (Tao et al., 2014a). The strong inter-species correlations (Fig. ~~S2a, 3b~~S3a, S3b) confirm the co-formation of $(NH_4)_2SO_4$ and NH_4NO_3 through gas-to-particle conversion processes. ~~The distinct~~ Revealed across distinct pollution episodes, the unique sulfur and oxygen isotopic signatures (Fig. 2b) provide unequivocal evidence of temporal shifts in sulfate formation pathways. To accurately deconvolute the relative contributions of these specific reaction routes, rigorous mechanistic modeling becomes indispensable. Crucially, the persistent incomplete oxidation of sulfur dioxide to sulfate under all pollution conditions (Fig. 2c) underscores the imperative for oxidation-process-constrained model optimization to elucidate the authentic atmospheric sulfate formation mechanisms.

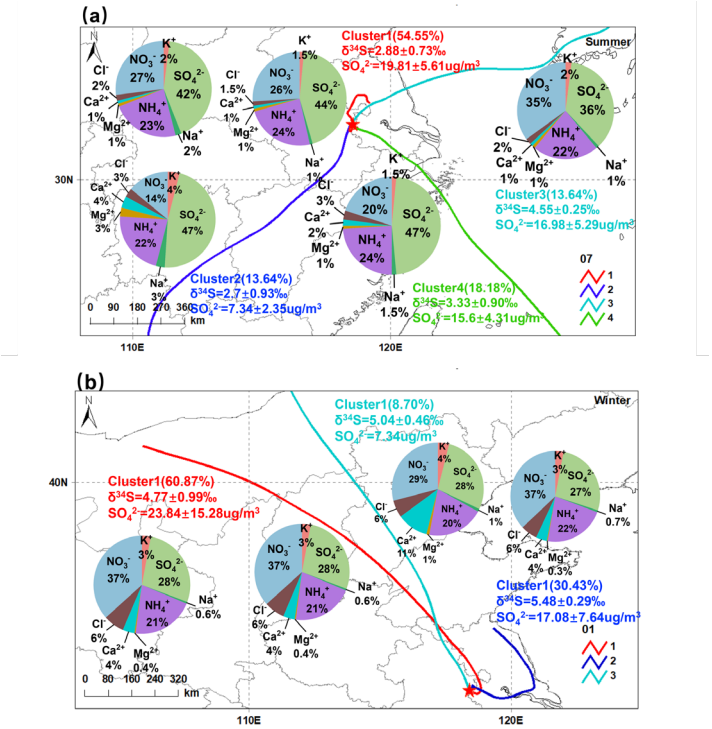

Figure 3. Pie charts of relative abundances of ions to TWSIIs and the values in Nanjing for the different air clusters. The concentrations of TWSIIs and the $\delta^{34}S-SO_4^{2-}$ values are shown in the parentheses. (a: winter b: summer)

The oxygen isotopic composition of atmospheric sulfate serves as a reliable indicator of oxidation pathways, with sulfate in $PM_{2.5}$ predominantly originating from SO_2 oxidation, consistent with established atmospheric chemistry. The $\delta^{34}S$-SO_4^{2-} values (+1.7‰ to +6.3‰) of Nanjing sulfate aerosols, indicating coal combustion (+4.6‰ to +6.6‰) as the dominant source, thereby reflecting a greater coal-derived contribution relative to other Chinese regions. Cluster analysis of air mass trajectories reveals distinct seasonal patterns. During summer (Fig. 3b), trajectories originating locally (54.55%), southwest China (13.64%), southeast China (18.18%), and the eastern Yellow Sea (13.64%) exhibit higher SO_4^{2-} concentrations locally (19.81 ± 5.61 μg m^{-3}) versus southwest (7.34 ± 2.35 μg m^{-3}), southeast (15.6 ± 4.31 μg m^{-3}), and Yellow Sea (16.98 ± 5.29 μg m^{-3}) sources, while $\delta^{34}S$-SO_4^{2-} values show an inverse trend with lower values locally (2.88 ± 0.73‰) and in the southwest (2.70 ± 0.93‰) compared to southeast (3.33 ± 0.9‰) and Yellow Sea regions (4.55 ± 0.25‰), suggesting heterogeneous sources and formation mechanisms. Winter measurements (Fig. 3a) display significant sulfate concentration disparities across back trajectories of air mass (e.g., cluster 1: 23.84 ± 15.28 μg m^{-3}; cluster 3: 7.34 μg m^{-3}), but statistically invariant $\delta^{34}S$-SO_4^{2-} values (cluster 1: 4.77 ± 0.99‰; cluster 3: 5.04 ± 0.46‰); ~~Northeastern Province~~ northeastern province (5.48 ± 0.29‰), with both concentration and $\delta^{34}S$ elevated versus summer, attributable to long-range transport of primary sulfates and coal-combustion emissions enriched in heavy isotopes. The significant negative correlation (Fig. 2b, 2d) between $\delta^{34}S$ and temperature arises as higher temperatures promote OH-mediated uniform oxidation, facilitating isotopic equilibrium fractionation during HSO_3^-/SO_4^{2-} exchange, which favors light-sulfur-isotope incorporation into sulfate and lowers summer $\delta^{34}S$ (Han et al., 2016; Novák et al., 2001). Thus, secondary sulfate formation pathways and source variations primarily drive the observed winter-high/summer-low $\delta^{34}S$ pattern in $PM_{2.5}$, underscoring the mechanistic study's critical role in sulfate pollution control.

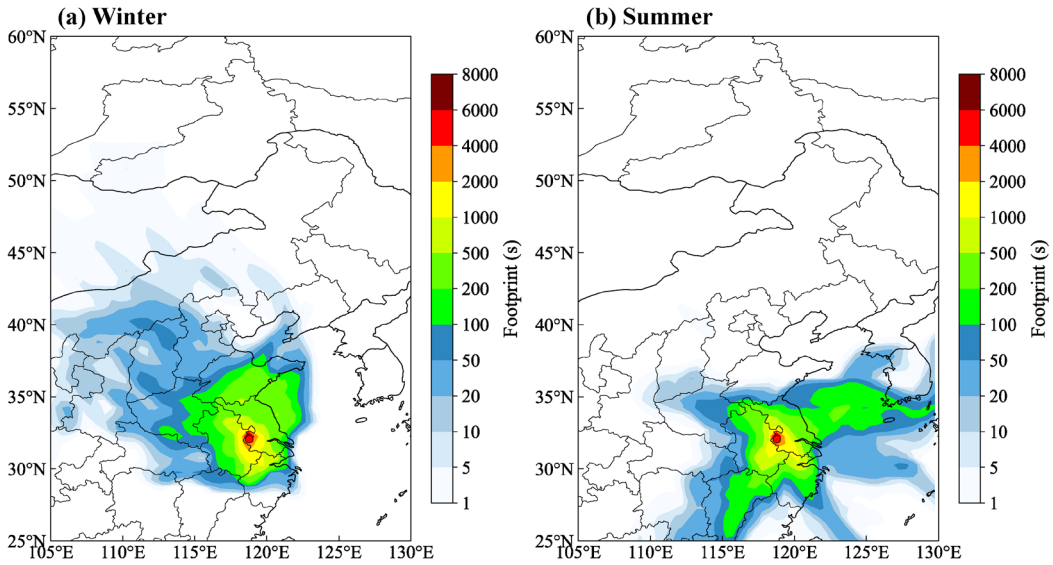

Figure 4. Footprints of sulfate aerosols at the receptor site during the (a) winter and (b) summer computed by the FLEXPART model. The color scale denotes the residence time (s) of sulfate aerosols in the grid cell.

Besides, by synergistically combining AMBTs (Fig. S4), CWT (Fig. S5) analysis, and FLEXPART footprint modeling (Fig. 4a, 4b), our integrated framework now successfully bridges the gap between empirical trajectory data and actual emission source strengths. This robust spatial validation explicitly supports our overarching objective to resolve long-standing discrepancies in atmospheric sulfate source attribution.

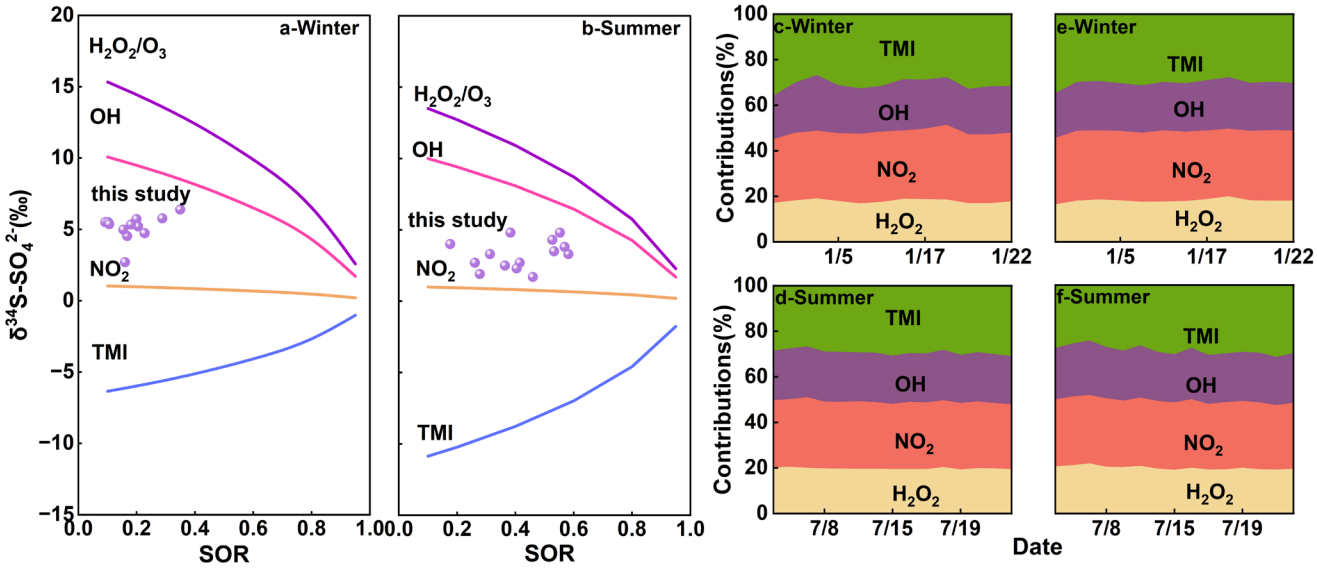

Figure 5. (a, b) Rayleigh fractionation models for secondary SO_4^{2-} formation in different seasons. (c, d, e, f) Relative contributions of primary, OH, TMI, NO_2, and H_2O_2/O_3 pathways to secondary SO_4^{2-} generation across different seasons. (c, d) represents the fractionation effects under InCO Process; (e, f) represents the fractionation effects under CO Process.

The atmospheric sulfate formation pathways exhibit distinct sulfur isotope fractionation signatures, as demonstrated by theoretical calculations of $\delta^{34}S\text{-}SO_4^{2-}$ evolution under different oxidation mechanisms ~~(Text. S2)~~. Complete oxidation of SO_2 via H_2O_2/O_3 pathways would drive $\delta^{34}S\text{-}SO_4^{2-}$ depletion from 15.3‰ to 2.6‰ (Fig. ~~4a~~5a), while OH-mediated oxidation would produce isotopic depletion from 11.8‰ to 3.4‰ (Fig. ~~4a~~5a), both scenarios reflecting progressive sulfur oxidation (SOR 0 to 1). Conversely, exclusive S(IV) + O_2 (TMI) pathway participation would generate $\delta^{34}S\text{-}SO_4^{2-}$ enrichment from -6.4‰ to -1.0‰ (Fig. 4a 5a). These differential fractionation patterns confirm the coexistence of multiple sulfate production routes in the atmosphere, with all observed $\delta^{34}S\text{-}SO_4^{2-}$ values falling within the predicted theoretical ranges. However, our field measurements demonstrate that total particulate sulfate concentrations peak at 27.55 ± 14.36 μg m^{-3} during severe haze events, which predominantly occur in winter. Consequently, when translating these relative fractions into absolute mass concentrations, the NO_2 pathway produces a substantially higher burden of particulate sulfate in winter compared to summer.

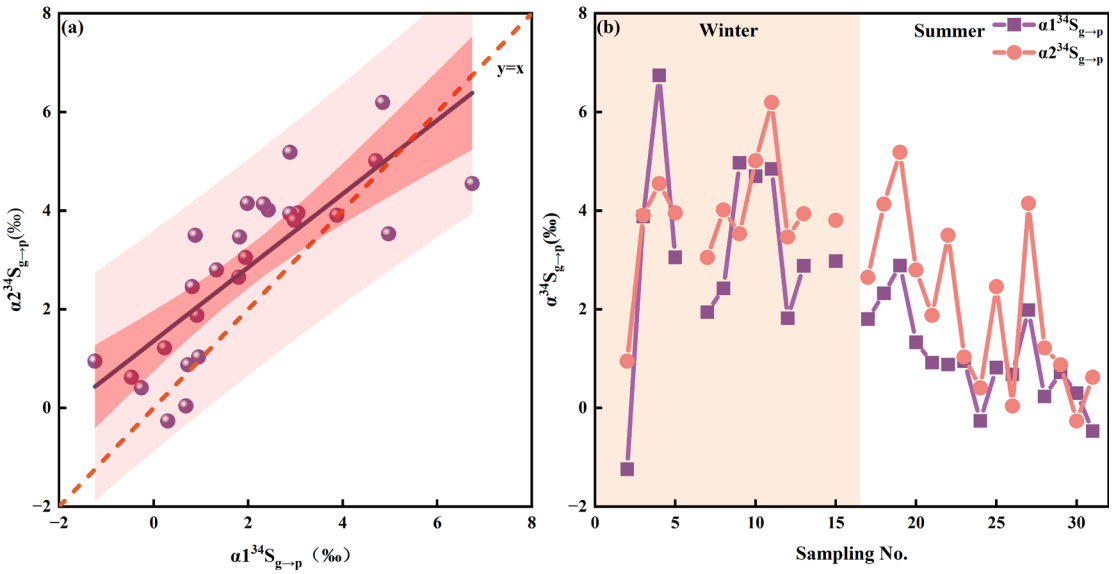

Figure 6. Linear regression between fractionation factor α1 (InCO Process) and fractionation factor α2 (CO Process). (The red line represents y = x [1:1 line], and the green line represents the fftted regression line between them.)

The isotopic fractionation factor α for sulfur isotopes was derived via Rayleigh fractionation models applied to δ^{34}S-$SO_{2\text{-emission}}$ calculations based on atmospheric δ^{34}S-SO_4^{2-} and SOR, with synchronous field measurements (InCO Process) of δ^{34}S-SO_2 averaging 1.7 ± 1.2‰ (range: -1.80 to +4.05‰), yielding $\alpha = 2.0 \pm 1.8$‰ (range: -1.2 to +6.7‰) (Fig. ~~5b~~ 6b) per designated formula. Under complete oxidation (CO Process) (SOR = 1), δ^{34}S-SO_4^{2-} demonstrated a significant negative correlation with SOR (δ^{34}S-SO_4^{2-} = -3.16 × SOR + 5.03=5.03; r = -0.36, p ≤ 0.05) (Fig. ~~S4~~S6), resulting in δ^{34}S-$SO_{2\text{-emission}}$ of 1.8‰ at full conversion, which exceeds values from Shanghai (1.3‰) (Li et al., 2020), Hangzhou (1.5‰) (Lin et al., 2022), and Jiaozuo (1.7‰) (Zheng et al., 2024) and represents the pre-transformation source signature. An alternative α calculation (formula 9) generated a mean of 2.8 ± 1.7‰ (range: -0.2 to +6.1‰), higher than Guangzhou (< 1.5‰) (Fan et al., 2020b) but lower than Beijing (4.2 ± 1.2‰) (Lin et al., 2018) with elevated α in ~~central~~ eastern China attributable to temperature-dependent fractionation increases (Fig. ~~S5~~ S7). The discrepancies arose from oxidation-rate variations under full-oxidation assumptions that alter pathway quantification.

~~Quantitative pathway apportionment of sulfate formation was achieved through systematic evaluation of reaction-specific α values derived for each SO_2 oxidation mechanism~~. By systematically evaluating the reaction-specific fractionation factors intrinsic to distinct SO_2 oxidation mechanisms, we successfully apportioned the diverse pathways governing sulfate formation. This ~~results~~ evaluation ~~demonstrate~~ reveals that TMI-catalyzed and NO_2-mediated reactions ~~oxidation pathways~~ collectively dictate atmospheric sulfate production across all considered ~~oxidation~~ scenarios. ~~Notably,~~ Crucially, ~~complete-oxidation assumptions systematically underestimate~~ as corroborated by isotopic mass balance calculations, imposing idealized complete-oxidation assumptions systematically suppresses the calculated contribution of the TMI pathway, ~~contribution compared to partial-oxidation models~~ a bias successfully resolved through the application of kinetic partial-oxidation models. ~~as revealed by isotopic mass balance calculations.~~ This systematic bias originates from neglecting kinetic fractionation effects during

intermediate oxidation stages, particularly under high aerosol acidity conditions where TMI chemistry prevails. The persistent dominance of these two pathways persists despite varying meteorological conditions and emission profiles, suggesting their fundamental role in sulfur cycling.

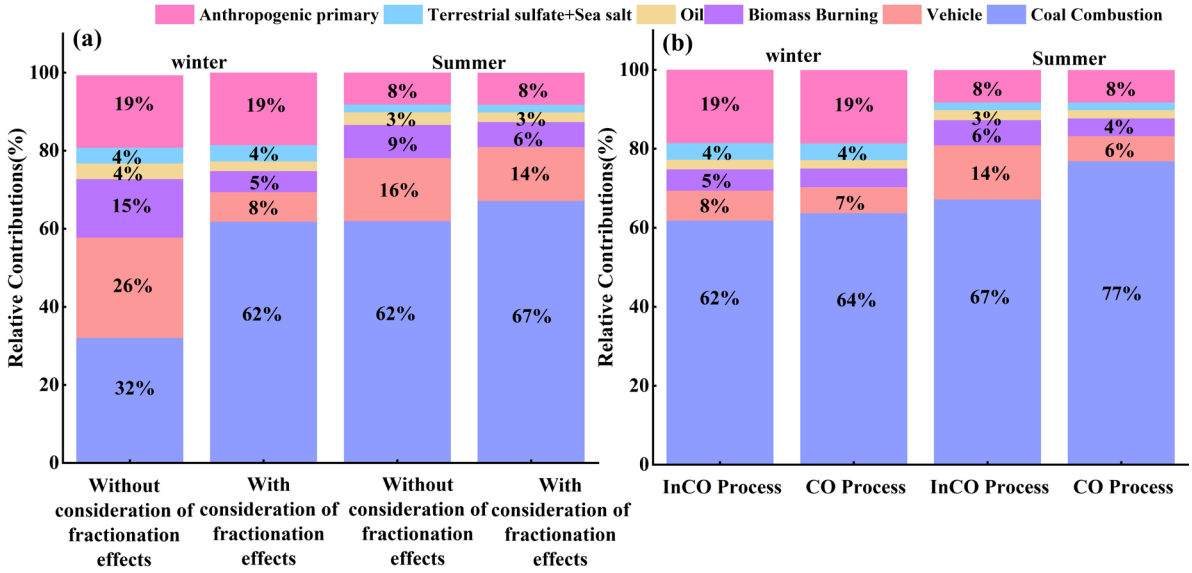

Figure 7. (a) Seasonal variations of source apportionments to sulfate aerosols in Nanjing. (b) Source apportionments of sulfate aerosols in Nanjing resolved by the SIAR model with consideration of fractionation effects under InCO Process and CO Process.

Quantitative source apportionment of atmospheric sulfate was achieved through coupled $\delta^{34}S\text{-}SO_4^{2-}$ measurements and Bayesian isotopic mixing models, requiring emission source-specific $\delta^{34}S$ signatures as critical input parameters. Correction for sulfur isotopic fractionation during SO_2 – to – SO_4^{2-} conversion is essential, as this process enriches $\delta^{34}S$ values by 1.2–7.2‰ (Lin et al., 2022), necessitating subtraction of pathway-specific fractionation coefficients prior to source quantification. Neglecting fractionation effects distorts source contributions, yielding winter estimates of 19% (anthropogenic primary sulfate), 4% (terrestrial sulfate and sea salt), 32% (coal), ~~5.2~~ 4% (oil), ~~20.1~~ 15% (biomass), and ~~33.3~~ 26% (vehicle), alongside summer values of ~~(68.9%, 3.6%, 9.5%, and 18.0%)~~ 8%, 2%, 62%, 3%, 9%, and 16% (Fig. ~~6a~~ 7a) respectively–results that inaccurately emphasize traffic emissions contrary to regional emission inventories and chemical transport modeling. Incorporating fractionation factors resolves this discrepancy, aligning sulfate sources with inventory data where coal combustion dominates annually, while idealized complete-oxidation models underestimate summer vehicle contributions by ~~8.2~~ 8% and overestimate coal combustion proportions (about ~~10.8~~10%) by comparable margins despite minimal winter deviations (Fig. ~~6b~~ 7b). This systematic validation underscores the requirement for fractionation correction in isotope-based atmospheric sulfate sourcing.

4 Conclusions

~~This study establishes a paradigm shift in atmospheric sulfate source apportionment by advancing beyond conventional isotopic models constrained by idealized SO_2 oxidation assumptions.~~ By transcending the idealized SO_2 oxidation assumptions that constrain conventional isotopic models, this study offers a critical advancement in atmospheric sulfate source

apportionment. ~~Through the integration of field-observed oxidation kinetics with optimized isotopic fractionation corrections, we demonstrate the predominance of TMI-catalyzed and NO_2-mediated pathways in sulfate formation, with coal combustion (summer overestimation: 10.8%) and traffic emissions (summer underestimation: 8.2%) (Fig.6b) identified as dominant sources. Crucially, comparative model analysis reveals systematic biases in traditional 220-complete-oxidation frameworks, which disproportionately diminish TMI pathway contributions while misallocating source-specific burdens.~~ Integrating field-observed oxidation kinetics with optimized fractionation corrections reveals the predominance of TMI-catalyzed and NO_2-mediated pathways–chemical realities that traditional complete-oxidation frameworks systematically obscure, thereby disproportionately diminishing TMI contributions and misallocating source-specific burdens. ~~These methodological reffnements enhancing the precision of stable isotope tracing techniques relative error margin, and reconciling long-standing discrepancies between isotopic, inventory-based, and transport-modeling approaches in particulate matter source attribution.~~ Crucially, correcting these systematic biases exposes a profound seasonal misalignment in current emission inventories, which overestimate coal combustion by 10% while underestimating traffic emissions by 8% during summer (Fig. ~~6b~~7b). Beyond reconciling long-standing discrepancies among isotopic, inventory-based, and transport-modeling approaches, these refinements carry immediate policy implications. ~~The validated framework provides actionable scientific basis for targeted emission control strategies, particularly in addressing combustion-related sulfate precursors across seasonal variations.~~ Specifically, they demonstrate that effective sulfate mitigation cannot rely solely on blanket SO_2 reductions; rather, regulatory frameworks must pivot toward multi-pollutant, seasonally differentiated strategies that dynamically target summer traffic dynamics and the co-emitted transition metals driving catalytic sulfate formation.

Code and data availability. Data used in this study are available upon request to the corresponding author. The data underlying the findings of this study are available from the corresponding author upon reasonable request. Global data assimilation system (GDAS) data were obtained from the multi-scale meteorological data set provided by the National Centers for Environmental Prediction in the United States (http://www.ready.noaa.gov/hypub-bin/trajtype.pl). The stable isotope mixing models in R is an upgraded version of the SIAR package, and it has many similar functionalities. This new version includes more complex mixing models and has advanced plotting capabilities (http://cran.r-project.org/web/packages/simmr/vignettes/simmr.html).

Author contributions. Z.-B.G. designed the research. X.-X.B. performed the model experiments. J.-Y.G. analyzed the data. Z.-Z.X. and Q.-W.A. conceptualization, methodology, software, investigation, funding acquisition, resources, data curation, validation, formal analysis. Q.-J.G. and S.-S.M. methodology, investigation, and software. X.-X.B. and P.-X.Q. prepared the manuscript and all co-authors helped improve the manuscript.

Competing interests. The authors declare no competing financial interest.

Disclaimer. Publisher's note: Copernicus Publications remains neutral with regard to jurisdictional claims made in the text, published maps, institutional affiliations, or any other geographical representation in this paper. The authors bear the ultimate responsibility for providing appropriate place names. Views expressed in the text are those of the authors and do not necessarily reflect the views of the publisher.

Acknowledgements. The authors acknowledge the financial support from the National Natural Science Foundation of China (grant no. 42473024).

Financial support. This work was supported by the National Natural Science Foundation of China (42473024).

References

Alexander, B., Park, R. J., Jacob, D. J., and Gong, S.: Transition metal-catalyzed oxidation of atmospheric sulfur: Global implications for the sulfur budget, J. Geophys. Res. Atmos., 114, D02309, https://doi.org/10.1029/2008JD010486, 2009.

Arimoto, R., Duce, R., Savoie, D., Prospero, J., Talbot, R., Cullen, J., Tomza, U., Lewis, N., and Ray, B.: Relationships among aerosol constituents from Asia and the North Pacific during PEM-West A, ~~Journal of Geophysical Research: Atmospheres~~ J. Geophys. Res. Atmos., 101, 2011–2023, https://doi.org/10.1029/95JD01071, 1996.

Chen, Z., Li, H., Shang, H., Liu, X., Guo, F., Liu, X., Yu, L., Zhou, B., Liu, X., Shi, Y., Zhang, L., and Ai, Z.: Oxalate-promoted SO_2 uptake and oxidation on iron minerals: Implications for secondary sulfate aerosol formation, Environ. Sci. Technol., 57, 13559–13568, https://doi.org/10.1021/acs.est.3c03369, 2023.

Dao, X., Lin, Y., Cao, F., Di, S., Hong, Y., Xing, G., Li, J., Fu, P., and Zhang, Y.: Introduction to the National Aerosol Chemical Composition Monitoring Network of China: Objectives, current status, and outlook, Bull. Amer. Meteorol. Soc., 100, ES337–ES351, https://doi.org/10.1175/BAMS-D-18-0325.1, 2019.

Dasari, S., and Widory, D.: Retrospective isotopic analysis of summertime urban atmospheric sulfate in South Asia using improved source constraints, ACS ES&T Air, 1, 357–364, https://doi.org/10.1021/acsestair.3c00060, 2024.

Dasari, S., Andersson, A., Stohl, A., Evangeliou, N., Bikkina, S., Holmstrand, H., Budhavant, K., Salam, A., and Gustafsson, Ö.: Source quantification of South Asian black carbon aerosols with isotopes and modeling, Environ. Sci. Technol., 54, 11771–11779, https://doi.org/10.1021/acs.est.0c02193, 2020.

Dasari, S., Paris, G., Saar, B., Pei, Q., Cong, Z., and Widory, D.: Sulfur Isotope Anomalies ($\Delta^{33}S$) in Urban Air Pollution Linked to Mineral-Dust-Associated Sulfate, Environ. Sci. Technol. Lett., 9, 604–610, https://doi.org/10.1021/acs.estlett.2c00312, 2022.

Ding, X., Li, Q., Wu, D., Wang, X., Li, M., Wang, T., Wang, L., and Chen, J.: Direct observation of sulfate explosive growth in wet plumes emitted from typical coal-fired stationary sources, Geophys. Res. Lett., 48, e2020GL092071, https://doi.org/10.1029/2020GL092071, 2021.

Fan, M., Zhang, Y., Lin, Y., Cao, F., Zhao, Z., Sun, Y., Qiu, Y., Fu, P., and Wang, Y.: Changes of emission sources to nitrate aerosols in Beijing after the clean air actions: Evidence from dual isotope compositions, ~~Journal of Geophysical Research: Atmospheres~~ J. Geophys. Res. Atmos., 125, e2019JD031998, https://doi.org/10.1029/2019JD031998, 2020a.

Fan, M., Zhang, Y., Lin, Y., Li, J., Cheng, H., An, N., Sun, Y., Qiu, Y., Cao, F., and Fu, P.: Roles of sulfur oxidation pathways in the variability in stable sulfur isotopic composition of sulfate aerosols at an urban site in Beijing, China, ~~Environmental Science & Technology~~ Environ. Sci. Technol. Lett., 7, 883–888, https://doi.org/10.1021/acs.estlett.0c00623, 2020b.

Fan, M., Hong, Y., Zhang, Y., Sha, T., Lin, Y., Cao, F., and Guo, H.: Increasing nonfossil fuel contributions to atmospheric nitrate in urban China from observation to prediction, Environ. Sci. Technol., 57, 18172–18182, https://doi.org/10.1021/acs.est.3c01651, 2023.

Guo, Z., Guo, Q., Chen, S., Zhu, B., Zhang, Y., Yu, J., and Guo, Z.: Study on pollution behavior and sulfate formation during the typical haze event in Nanjing with water soluble inorganic ions and sulfur isotopes, ~~Atmospheric Research~~ Atmos. Res., 217, 198–207, https://doi.org/10.1016/j.atmosres.2018.11.009, 2019.

Guo, Z., Lu, K., Qiu, P., Xu, M., and Guo, Z.: Quantifying SO_2 oxidation pathways to atmospheric sulfate using stable sulfur and oxygen isotopes: laboratory simulation and field observation, Atmos. Chem. Phys., 24, 2195–2205, https://doi.org/10.5194/acp-24-2195-2024, 2024.

Han, X., Guo, Q., Liu, C., Fu, P., Strauss, H., Yang, J., Hu, J., Wei, L., Ren, H., Peters, M., Wei, R., and Tian, L.: Using stable isotopes to trace sources and formation processes of sulfate aerosols from Beijing, China, ~~Scientific Reports~~ Sci. Rep., 6, 29958, https://doi.org/10.1038/srep29958, 2016.

Han, X., Lang, Y., Guo, Q., Li, X., Ding, H., and Li, S.: Enhanced oxidation of SO_2 by H_2O_2 during haze events: constraints from sulfur isotopes, ~~Journal of Geophysical Research: Atmospheres~~ J. Geophys. Res. Atmos., 127, e2022JD036960, https://doi.org/10.~~1073/pnas.2408199121~~1029/2022JD036960, 2022.

Harris, E., Sinha, B., Hoppe, P., Crowley, J., Ono, S., and Foley, S.: Sulfur isotope fractionation during oxidation of sulfur dioxide: gas-phase oxidation by OH radicals and aqueous oxidation by H_2O_2, O_3 and iron catalysis, ~~Atmospheric Chemistry and Physics~~ Atmos. Chem. Phys., 12, 407–423, https://doi.org/10.5194/acp-12-407-2012, 2012a.

Harris, E., Sinha, B., Hoppe, P., Foley, S., and Borrmann, S.: Fractionation of sulfur isotopes during heterogeneous oxidation of ~~SO 2~~SO_2 on sea salt aerosol: a new tool to investigate non-sea salt sulfate production in the marine boundary layer,

~~Atmospheric Chemistry and Physics~~ Atmos. Chem. Phys., 12, 4619–4631, https://doi.org/10.5194/acp-12-4619-2012, 2012b.

~~Sinha, B.,~~ Harris, E., Sinha, B., Hoppe, P., and Ono, S.: High-precision measurements of ^{33}S and ^{34}S fractionation during SO_2 oxidation reveal causes of seasonality in SO_2 and sulfate isotopic composition, Environ. Sci. Technol., 47, 12174–12183, https://doi.org/10.1021/es402824c, 2013a.

Harris, E., Sinha, B., van Pinxteren, D., Tilgner, A., Fomba, K. W., Schneider, J., Roth, A., Gnauk, T., Fahlbusch, B., Mertes, S., Lee, T., Collett, J., Foley, S., Borrmann, S., Hoppe, P., and Herrmann, H.: Enhanced role of transition metal ion catalysis during in-cloud oxidation of SO_2, Science, 340, 727–730, https://doi.org/10.1126/science.1230911, 2013b.

He, K., Zhao, Q., Ma, Y., Duan, F., Yang, F., Shi, Z., and Chen, G.: Spatial and seasonal variability of $PM_{2.5}$ acidity at two Chinese megacities: insights into the formation of secondary inorganic aerosols, Atmos. Chem. Phys., 12, 1377–1395, https://doi.org/10.5194/acp-12-1377-2012, 2012.

He, P., Alexander, B., Geng, L., Chi, X., Fan, S., Zhan, H., Kang, H., Zheng, G., Cheng, Y., Su, C., Liu, C., and Xie, Z.: Isotopic constraints on heterogeneous sulfate production in Beijing haze, Atmos. Chem. Phys., 18, 5515–5528, https://doi.org/10.5194/acp-18-5515-2018, 2018.

Kang, Y., Liu, M., Song, Y., Huang, X., Yao, H., Cai, X., Zhang, H., Kang, L., Liu, X., Yan, X., He, H., Zhang, Q., Shao, M., and Zhu, T.: High-resolution ammonia emissions inventories in China from 1980 to 2012, ~~Atmospheric Chemistry and Physics~~ Atmos. Chem. Phys., 16, 2043–2058, https://doi.org/10.5194/acp-16-2043-2016, 2016.

Li, J., Zhang, Y., Cao, F., Zhang, W., Fan, M., Lee, X., and Michalski, G.: Stable sulfur isotopes revealed a major role of transition-metal ion-catalyzed SO_2 oxidation in haze episodes, ~~Environmental Science & Technology,~~ Environ. Sci. Technol., 54, 2626–2634, https://doi.org/10.1021/acs.est.9b07150, 2020.

~~Mang, L., Xiaolin, Z., Menghan, L., Yilun, X., Zhisheng, Z., Jun, T., Binbin, S., Lanzhong, L., Yanan, S., and Thiemens, M. H.~~ Lin, M., Zhang, X., Li, M., Xu, Y., Zhang, Z., Tao, J., Su, B., Liu, L., Shen, Y., and Thiemens, M. H.: Five-S-isotope evidence of two distinct mass-independent sulfur isotope effects and implications for the modern and Archean atmospheres, Proc. Natl. Acad. Sci., 115, 8541–8546, https://doi.org/10.1073/pnas.1803420115, 2018.

Lin, Y., Yu, M., Xie, F., and Zhang, Y.: Anthropogenic emission sources of sulfate aerosols in Hangzhou, East China: insights from isotope techniques with consideration of fractionation effects between gas-to-particle transformations, Environ. Sci. Technol., 56, 3905–3914, https://doi.org/10.1021/acs.est.1c05823, 2022.

Lin, Y., Fan, M., Yu, M., Abulimiti, A., Xie, F., Xu, R., and Zhang, Y.: Significant contributions of regional transport to sulfate aerosols during haze events in northern China Plain: constrained by sulfur isotopic compositions, J. Geophys. Res. Atmos., 130, e2025JD043716, https://doi.org/10.1029/2025JD043716, 2025.

Ma, J., Chen, B., He, Q., Yan, X., Wang, G., Cheng, S., Steil, B., Brühl, C., Pozzer, A., and Lelieveld, J.: Modelling the deep convective transport of trace gases (CO, NH_3 and SO_2) from the planetary boundary layer to the Asian summer monsoon anticyclone, EGUsphere [preprint], https://doi.org/10.5194/egusphere-2025-5587, 2025.

Mizutani, Y., and Rafter, T.: Oxygen isotopic composition of sulphates. Part 4. Bacterial fractionation of oxygen isotopes in the reduction of sulphate and in the oxidation of sulphur, N. Z. J. Sci., 12: 60–8, https://www.osti.gov/biblio/4764537, 1969.

Mukai, H., Tanaka, A., Fujii, T., Zeng, Y., Hong, Y., Tang, J., Guo, S., Xue, H., Sun, Z., Zhou, J., Xue, D., Zhao, J., Zhai, G., Gu, J., and Zhai, P.: Regional characteristics of sulfur and lead isotope ratios in the atmosphere at several Chinese urban sites, Environ. Sci. Technol., 35, 1064–1071, https://doi.org/10.1021/es001399u, 2001.

Novák, M., Jačková, I., and Přechová, E.: Temporal trends in the isotope signature of air-borne sulfur in Central Europe, ~~Environmental science & technology~~ Environ. Sci. Technol., 35, 255–260, https://doi.org/10.1021/es0000753, 2001.

Parnell, A. C., Inger, R., Bearhop, S., and Jackson, A. L.: Source partitioning using stable isotopes: coping with too much variation, PLOS ONE., 5, e9672, https://doi.org/10.1371/journal.pone.0009672, 2010.

Ruan, X., Zhao, C., Zhou, T., Zhang, Z., Ma, T., Wang, X., Zhao, W., Su, G., and Geng, L.: Cloud and aerosol chemistry together explain the high sulfate aerosol content in a heavy haze episode in Central Eastern China, Environ. Sci. Technol., 59, 23398–23409, https://doi.org/10.1021/acs.est.5c07415, 2025.

Tanaka, N., Rye, D. M., Xiao, Y., and Lasaga, A. C.: Use of stable sulfur isotope systematics for evaluating oxidation reaction pathways and in-cloud-scavenging of sulfur dioxide in the atmosphere, Geophys. Res. Lett., 21, 1519–1522, https://doi.org/10.1029/94GL00893, 1994.

Tao, J., Gao, J., Zhang, L., Zhang, R., Che, H., Zhang, Z., Lin, Z., Jing, J., Cao, J., and Hsu, S.: $PM_{2.5}$ pollution in a megacity of southwest China: source apportionment and implication, ~~Atmospheric Chemistry and Physics~~ Atmos. Chem. Phys., 14, 8679–8699, https://doi.org/10.5194/acp-14-8679-2014, 2014a.

Tao, J., Zhang, L., Ho, K., Zhang, R., Lin, Z., Zhang, Z., Lin, M., Cao, J., Liu, S., and Wang, G.: Impact of $PM_{2.5}$ chemical compositions on aerosol light scattering in Guangzhou—the largest megacity in South China, ~~Atmospheric Research~~ Atmos. Res., 135, 48–58, https://doi.org/10.1016/j.atmosres.2013.08.015, 2014b.

Tao, Y., Ye, X., Ma, Z., Xie, Y., Wang, R., Chen, J., Yang, X., and Jiang, S.: Insights into different nitrate formation mechanisms from seasonal variations of secondary inorganic aerosols in Shanghai, Atmos. Environ., 145, 1–9, https://doi.org/10.1016/j.atmosenv.2016.09.012, 2016.

Wang, G., Zhang, R., Gomez, M. E., Yang, L., Levy Zamora, M., Hu, M., Lin, Y., Peng, J., Guo, S., Meng, J., Li, J., Cheng, C., Hu, T., Ren, Y., Wang, Y., Gao, J., Cao, J., An, Z., Zhou, W., Li, G., Wang, J., Tian, P., Marrero-Ortiz, W., Secrest, J., Du, Z., Zheng, J., Shang, D., Zeng, L., Shao, M., Wang, W., Huang, Y., Wang, Y., Zhu, Y., Li, Y., Hu, J., Pan, B., Cai, L., Cheng, Y., Ji, Y., Zhang, F., Rosenfeld, D., Liss, P. S., Duce, R. A., Kolb, C. E., and Molina, M. J.: Persistent sulfate for-mation from London Fog to Chinese haze, P. Natl. Acad. Sci. USA, 113, 13630–13635, https://doi.org/10.1073/pnas.1616540113, 2016.

Wang, J., Li, J., Ye, J., Zhao, J., Wu, Y., Hu, J., Liu, D., Nie, D., Shen, F., Huang, X., Huang, D., Ji, D., Sun, X., Xu, W., Guo, J., Song, S., Qin, Y., Lin, P., Turner, J., Lee, H., Hwang, S., Liao, H., Martin, S., Zhang, Q., Chen, M., Sun, Y., Ge, X., and Jacob, D.: Fast sulfate formation from oxidation of SO_2 by NO_2 and HONO observed in Beijing haze, Nat. Commun., 11, 2844, https://doi.org/10.1038/s41467-020-16683-x, 2020.

Wang, W., Yu, J., Cui, Y., He, J., Xue, P., Cao, W., Ying, H., Gao, W., Yan, Y., Hu, B., Xin, J., Wang, L., Liu, Z., Sun, Y., Ji, D., and Wang, Y.: Characteristics of fine particulate matter and its sources in an industrialized coastal city, Ningbo, Yangtze River Delta, China, Atmos. Res., 203, 105–117, https://doi.org/10.1016/j.atmosres.2017.11.033, 2018.

Wei, L., Yue, S., Zhao, W., Yang, W., Zhang, Y., Ren, L., Han, X., Guo, Q., Sun, Y., Wang, Z., and Fu, P.: Stable sulfur isotope ratios and chemical compositions of fine aerosols ($PM_{2.5}$) in Beijing, China, Sci. Total Environ., 633, 1156–1164, https://doi.org/10.1016/j.scitotenv.2018.03.153, 2018.

Xiao, H., Xiao, H., Long, A., Wang, Y., and Liu, C.: Sources and meteorological factors that control seasonal variation of $\delta^{34}S$ values in rainwater, ~~Atmospheric research~~ Atmos. Res., 149, 154–165, https://doi.org/10.1016/j.atmosres.2014.06.003, 2014.

Yanagisawa, F., and Sakai, H.: Thermal decomposition of barium sulfate-vanadium pentoxide-silica glass mixtures for preparation of sulfur dioxide in sulfur isotope ratio measurements, Anal. Chem., 55, 985–987, https://doi.org/10.1021/ac00257a046, 1983.

Yang, R., Lou, Q., Wang, M., Cao, L., and Luo, L.: Using stable sulfur isotopes to quantify the formation mechanism and sources of SO_4^{2-} in $PM_{2.5}$ in Haikou City, ~~ACS Earth and Space Chemistry~~ ACS Earth Space Chem., 9, 560–568, https://doi.org/10.1021/acsearthspacechem.4c00304, 2025.

Yao, X., Chan, C. K., Fang, M., Cadle, S., Chan, T., Mulawa, P., He, K., and Ye, B.: The water-soluble ionic composition of $PM_{2.5}$ in Shanghai and Beijing, China, ~~Atmospheric Environment~~ Atmos. Environ., 36, 4223–4234, https://doi.org/10.1016/S1352-2310(02)00342-4, 2002.

Yu, C., Liu, T., Chi, X., Huang, X., and Ding, A.: Salting-in of HCHO sustains fast hydroxymethanesulfonate formation in deliquesced sulfate aerosols, Environ. Sci. Technol. Lett., 13, 744–750, https://doi.org/10.1021/acs.estlett.6c00300, 2026.

Zhang, R., and Chan, C. K.: Simultaneous formation of sulfate and nitrate via co-uptake of SO_2 and NO_2 by aqueous NaCl droplets: combined effect of nitrate photolysis and chlorine chemistry, EGUsphere [preprint], https://doi.org/10.5194/egusphere-2023-223, 2023.

Zhang, X., Liu, J., Li, H., Zuo, Y., Zhang, C., Su, Z., Wang, S., Zhang, P., Chu, B., and He, H.: pH-dependent Fe(III) speciation and concerted proton–electron transfer mechanism accelerated S(IV) oxidation at the air–water interface, J. Am. Chem. Soc., 148, 11812–11821, https://doi.org/10.1021/jacs.5c21077, 2026.

Zheng, M., Song, D., Zhang, D., Cao, Y., and Fan, H.: Using sulfur isotopes to constrain the sources of sulfate in $PM_{2.5}$ during the winter in Jiaozuo City, Atmos. Environ., 332, 120618, https://doi.org/10.1016/j.atmosenv.2024.120618, 2024.